

Automatic extraction of wind erosion obstacles by integration of GIS data, DSM and stereo images

Y. ZHANG*†, C. HEIPKE‡, M. BUTENUTH‡ and X. HU†

†School of Remote Sensing and Information Engineering, Wuhan University, China

‡Institute of Photogrammetry and GeoInformation, University of Hannover, Germany

(Received 6 December 2004; in final form 10 October 2005)

Integrating multiple data sources is a very important strategy to obtain relevant solutions in geo-scientific analysis. This paper mainly deals with the integration of Geographical Information System (GIS) data, stereo aerial imagery and a Digital Surface Model (DSM) to extract wind erosion obstacles (namely tree rows and hedges) in open landscapes. Different approaches, such as image segmentation, edge extraction, linking, grouping and 3-dimensional verification with the DSM, are combined to extract the objects of interest. Experiments show that most wind erosion obstacles can be successfully extracted by the developed system.

1. Introduction

Wind erosion removes valuable topsoil containing organic matter and nutrients, which are essential for crop growth. It is a menace to the farming lands (Driehuyzen 2003). For example, desertification affected lands caused by wind erosion occupy 1 834 000 km² of China (UNCCD 2002). In Ontario, Canada, wind erosion has also been identified as the most serious land degradation problem (Wall *et al.* 2004). However, adequate wind erosion obstacles (or shelterbelts) can decrease wind speed and protect farming lands from being destroyed, so the extraction of wind erosion obstacles is useful for protecting the farming lands.

To facilitate automatic object extraction from aerial imagery, use of prior knowledge is advantageous (Heipke *et al.* 2000, Baltasvias 2004). Although considerable results have been achieved in the extraction of individual trees (Gougeon 1995, Pollock 1996, Dralle and Rudemo 1997, Larsen and Rudemo 1998, Wulder *et al.* 2000, Straub 2003, Koukoulas and Blackburn 2005), the extraction of vegetation, especially wind erosion obstacles using high-resolution imagery, is still at an early stage. The general idea of extracting wind erosion obstacles is addressed by Butenuth (2004). However, no experimental results have been presented. Preliminary results of extracting wind erosion obstacles are presented by Zhang (2004): by using data integration techniques, a large number of wind erosion obstacles can be automatically extracted.

Digital colour infrared (CIR) imagery is very important for data acquisition and updating, especially for vegetation (Lyon *et al.* 1998). The Normalized Difference

Most of this work was carried out while the corresponding author was with the Institute of Photogrammetry and GeoInformation, University of Hannover, Germany.

*Corresponding author. Email: zhangyj@whu.edu.cn, yongjun_zhang@hotmail.com

Vegetation Index (NDVI) is widely used in remote sensing applications, such as monitoring of vegetation condition and production (Lyon *et al.* 1998), extraction of trees in urban areas (Straub 2003), and relations between NDVI and tree productivity (Wang *et al.* 2004). The device type independent colour space CIE L^*a^*b was announced by the Commission Internationale de l'Eclairage (CIE) in 1976. It is mostly used for image analysis and industrial applications (e.g. Campadelli *et al.* 2000, Lebrun and Toussaint 2000, Lucchese and Mitra 2001) in the computer vision community.

This paper mainly deals with the automatic extraction of wind erosion obstacles in open landscapes using a data integration technique. The general strategy and test data sources are described. Afterwards, detailed methodology, including image segmentation, edge extraction and linking, edge grouping and matching, and verification with a Digital Surface Model (DSM), which contains the terrain elevations including all topographic objects like houses and trees, is discussed. The experimental results of RGB image segmentation with CIE L^*a^*b and the automatically extracted wind erosion obstacles are then given.

2. General strategy and data sources

2.1 General strategy

The purpose of the current research is to extract wind erosion obstacles by integrating GIS data, CIR stereo imagery with camera parameters as well as a DSM for potential application of soil monitoring and preservation. The related topics, such as semantic modelling (Butenuth 2004) or the helpful extraction of field boundaries (Butenuth and Heipke 2005) are not of interest in this paper. The work flow of extracting wind erosion obstacles is shown in figure 1. First, non-vegetation areas are removed by image segmentation techniques. Second, image features of tree rows and hedges are extracted with the Canny edge detector (Canny 1986). Edges corresponding to non-interesting regions, such as buildings and forests, are masked out by projecting the GIS data onto the image with known camera parameters. The remaining edges are linked, grouped and matched in turn. A DSM is also used in the grouping process because the distance between an adjacent hedge and tree row is usually very short. Then the matched edges are projected onto the landscape to obtain 3-dimensional edges with the known camera parameters of the stereo. Height information provided by the DSM is used to verify the potential wind erosion obstacles since they are higher than the landscape. Finally, the extracted wind erosion obstacles are described by their geometric properties (position, width and height).

2.2 Test data sources

GIS data with a geometric accuracy of approximately 3.0m represent the initial scene. Since only wind erosion obstacles are of interest, regions where no hedges and tree rows exist (e.g. urban, water, forest) in the imagery can be masked out by the GIS data. Figure 2 shows the GIS data superimposed onto an image in the open landscape. Settlements are depicted in white, and forests in green. A representative region is highlighted by the dashed white lines, and separately shown in figure 3.

CIR images with 0.5 m ground resolution are generated in August. Wind erosion obstacles show high grey values in the infrared channel, while crops show significantly less reflection. This information is advantageous for extracting the

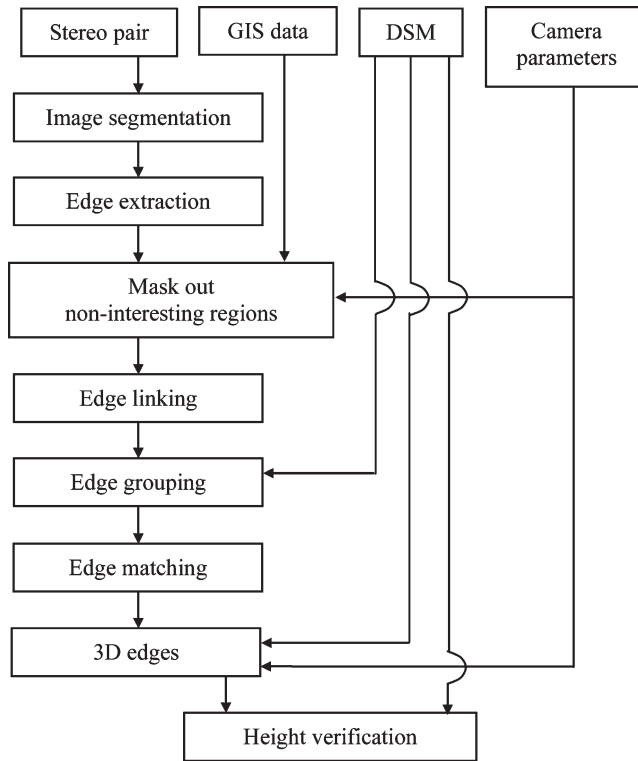


Figure 1. Flow chart for extracting wind erosion obstacles.

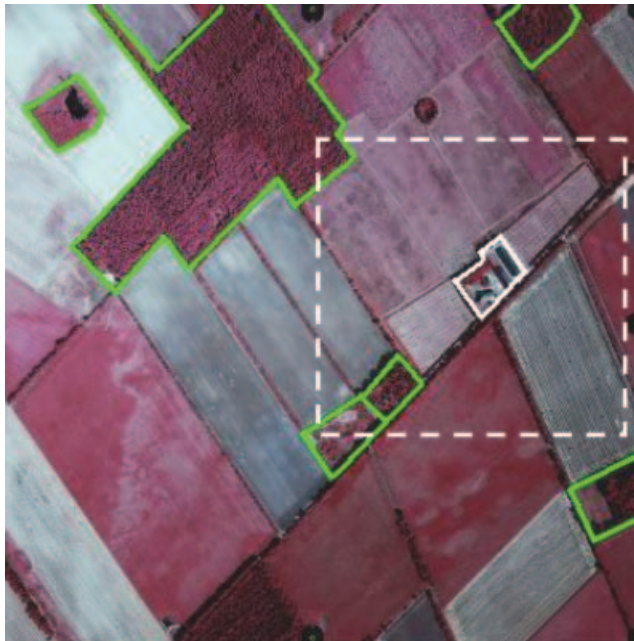


Figure 2. Open landscape with superimposed GIS data: forest boundaries (green), settlements (white).



Figure 3. Selected region of interest.

objects of interest automatically. For this task the colour space CIE L^*a^*b is used. The original CIR images are first mapped into RGB colour space using the standard procedure (infrared to red, red to green, green to blue); RGB is then transformed into colour space CIE L^*a^*b . Afterwards, the transformed image is segmented into vegetation and non-vegetation regions. It is true that grasslands also reflect strongly in the infrared channel. This means that the use of GIS data and CIR imagery is not reliable enough to extract wind erosion obstacles.

Additionally, a DSM with a 0.5 m ground resolution of the area of interest is generated using the commercial software package *VirtuoZo* (Supresoft 2004) with the CIR imagery and ground control points selected from the GIS data. The procedure of DSM generation mainly consists of aerial triangulation, image matching and model mosaicking. This procedure is similar to that of most current digital photogrammetric workstations (DPWs). Figure 4 shows the image draped over the generated DSM. As can be seen the area is mostly flat, only a few minor matching artefacts are visible. The wind erosion obstacles are clearly visible, as they are higher than the landscape. Thus, height information from the DSM is helpful for our task. It can be used together with GIS data and colour information to support the extraction of wind erosion obstacles.

3. Methodology of extraction of wind erosion obstacles

3.1 *Image segmentation*

There are many methods that can be used for image segmentation. The NDVI is one of the most widely used indices for differentiating between vegetation and non-vegetation areas in remote sensing. CIE L^*a^*b is very popular for image segmentation in computer vision.



Figure 4. Digital Surface Model (DSM) superimposed with orthoimage.

3.1.1 Segmentation by NDVI and similar vegetation indices. The use of image segmentation by NDVI for CIR images in order to extract vegetation is a well-known approach (e.g. Lyon *et al.* 1998, Butenuth 2004). NDVI calculations are based on the principle that actively growing green plants strongly absorb radiation in the red channel of the visible spectrum, while strongly reflecting radiation in the near infrared channel. The NDVI values vary from -1 to $+1$ and close to $+1$ for the strongest vegetative growth.

In case a near infrared channel is not available, as in the case for RGB images, the difference in reflection between the red and the green channel can be used to calculate a so called ‘greenness’ index (e.g. Niederöst 2003). The formal structure for computing this index is identical to the one for the NDVI, but the value of the green channel takes the place of the value of the infrared channel. Since the reflection difference between red and green is usually smaller than between red and infrared, the greenness index is less suited to the task at hand compared to the NDVI. Therefore, the greenness index is not further pursued in our work.

For the NDVI, the threshold for vegetation extraction is usually positive and near to zero, it may vary from 0.05 to 0.15. Human supervision is helpful for selecting the best threshold from typical imagery. For our test data, non-vegetation areas are not well removed with a threshold of 0.0, while many hedge areas are falsely removed with a threshold of 0.2. The best result is obtained with a threshold of 0.1. In order to keep all potential wind erosion obstacles in the segmented image, the threshold $NDVI=0.1$ is adopted. Figure 5 shows the segmentation results for the image depicted in figure 3. The white areas in the image are non-vegetation ones. As can be seen, the results of segmentation in the upper-left part are not satisfying. Some non-vegetation areas still exist in the image. Furthermore, the uninteresting field boundaries in the upper left part are very clear, while the wind erosion obstacles are

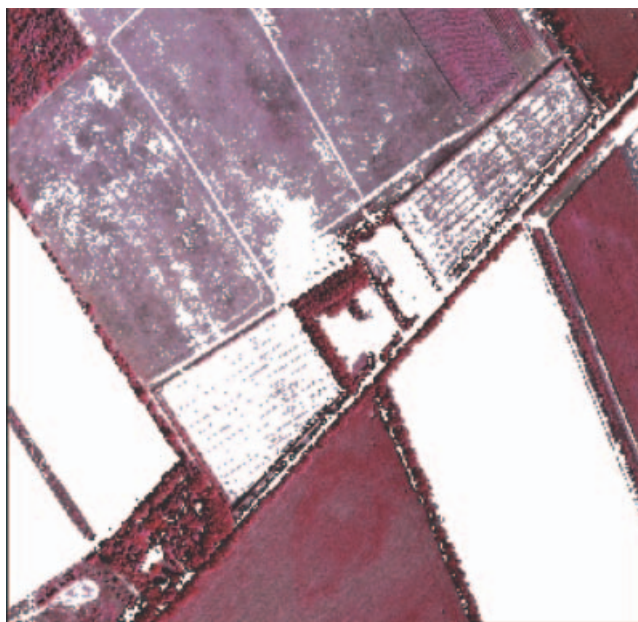


Figure 5. Result of segmentation by Normalised Difference Vegetation Index (NDVI).

not clearly distinguished from the background, for example in the right part of figure 5.

3.1.2 Segmentation by CIE $L^*a^*b^*$. There is no direct relation between RGB and CIE $L^*a^*b^*$. The transformation from RGB to CIE $L^*a^*b^*$ must be made indirectly via CIE XYZ. First, RGB is transformed into CIE XYZ, and then the received point is transformed into CIE $L^*a^*b^*$.

The CIE XYZ colour space was presented by CIE in 1931 (SEII 2002). Three axes X , Y and Z are orthogonally defined by the basic colours R , G and B (red, green and blue). Generally, only points in the surface $X + Y + Z = 1$ are considered. Each RGB point can be transformed into colour space CIE XYZ as follows (SEII 2002):

$$\begin{bmatrix} X \\ Y \\ Z \end{bmatrix} = \begin{bmatrix} 0.412291 & 0.357664 & 0.180209 \\ 0.212588 & 0.715329 & 0.072084 \\ 0.019326 & 0.119221 & 0.949102 \end{bmatrix} \begin{bmatrix} R \\ G \\ B \end{bmatrix} = M \begin{bmatrix} R \\ G \\ B \end{bmatrix} \quad (1)$$

In colour space CIE $L^*a^*b^*$, component L^* represents the lightness that varies from black (with value 0) to white (with value 100). The components a^* and b^* represent colour: a^* varies from green (with value -120) to red (with value $+120$), b^* varies from blue (with value -120) to yellow (with value $+120$). The transformation from CIE XYZ to CIE $L^*a^*b^*$ can be written as:

$$\begin{aligned} L &= 116(Y/W_y)^{1/3} - 16 && \text{if } 0.008856 < (Y/W_y) \\ L &= 903.3(Y/W_y) && \text{else} \end{aligned} \quad (2)$$

$$\begin{aligned} a &= 500(F(X/W_x) - F(Y/W_y)) \\ b &= 200(F(Y/W_y) - F(Z/W_z)) \end{aligned} \quad (3)$$

where (X, Y, Z) is the point to be converted, which can be obtained from equation (1), and (W_x, W_y, W_z) is the so called white point with $W_x=0.312779$, $W_y=0.329184$ and $W_z=0.358037$. Let p represent X/W_x , Y/W_y , and Z/W_z respectively, then $F(p)=p^{1/3}$ if $p>0.008856$, otherwise $F(p)=7.787*p+16/116$.

For CIR imagery, a^* is positive and close to +120 for the strongly reflecting vegetation. The segmentation result of figure 3 by CIE L^*a^*b with threshold $a^*=12$ (equivalent to $NDVI=0.1$, since $12/120=0.1$) is shown in figure 6. When compared with figure 5, it can be seen that more non-vegetation regions are removed. The non-interesting borders of fields, which are very clear at the upper-left part of figure 5, are completely removed. Furthermore, regions of wind erosion obstacles are well kept. They often exhibit very good edge structures, for example in the centre and right part of figure 6.

Many experiments have been carried out to compare the performance of image segmentation between NDVI and CIE L^*a^*b . All results are similar to the ones described above. So the CIE L^*a^*b approach is used for vegetation extraction in this paper. Another reason is that using CIE L^*a^*b , vegetation can also be extracted from RGB images because the component a^* is negative for vegetation in standard RGB imagery and close to -120 for green vegetation. To segment RGB imagery with CIE L^*a^*b , a^* from -0.15 to -0.05 should be applied as a threshold. The best threshold can again be obtained under human supervision. Meanwhile, it is of course not possible for NDVI to deal with RGB imagery: as mentioned a different vegetation index must be used.

3.1.3 Edge extraction and linking. Wind erosion obstacles, no matter whether they are tree rows or hedges, usually appear as linear features in the image, or they can be treated as a combination of edge segments. In this paper, the Canny edge detector

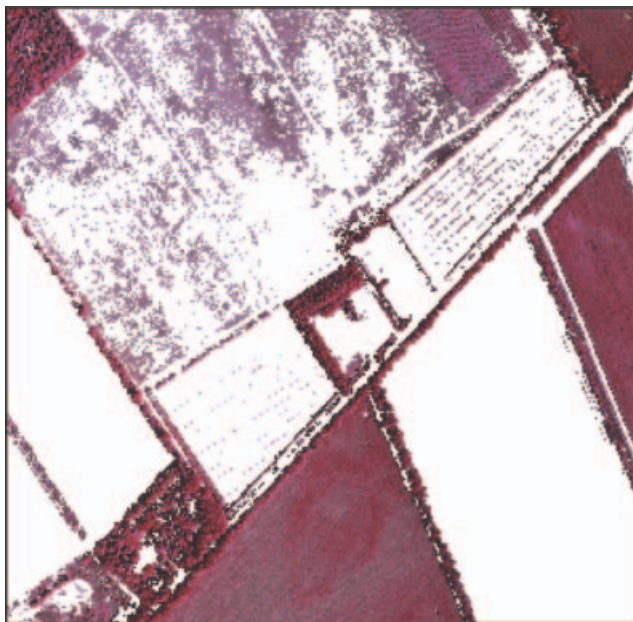


Figure 6. Result of segmentation by CIE L^*a^*b .

(Canny 1986) is used to extract these edges. In a pre-processing step, the image is smoothed by Gaussian convolution. Then, a two-dimensional first derivative operator is applied to the smoothed image to highlight regions of the image with high first spatial derivatives. Edges give rise to ridges in the resulting gradient magnitude image. Afterwards, the algorithm tracks these edges and sets all pixels not on the ridge top to zero, so as to give a thin edge in the output, a process known as non-maximum suppression. The tracking process exhibits hysteresis controlled by two thresholds: T_1 and T_2 where $T_1 > T_2$. Tracking can only begin at a point on a ridge higher than T_1 . Tracking then continues in both directions from that point until the height of the ridge falls below T_2 . This hysteresis helps to ensure that noisy edges are not broken up into multiple edge fragments. To this end, the extracted edges are converted into edge segments longer than a given length, such as 30 pixels in the image. In general, corresponding borders of most wind erosion obstacles can be extracted successfully.

Edges of non-interesting regions, such as forests and buildings, can be masked out with the available GIS data. Edges of field boundaries can be removed by CIE L^*a^*b . But it is very difficult to remove the boundaries of grassland because they also appear as clear linear features with a positive a^* value. On the other hand, wind erosion obstacles are sometimes connected to grassland. Therefore, all remaining edges have to be treated as potential wind erosion obstacles at this stage.

Subsequently, the remaining edge segments are linked in the along-edge-direction by their inclination, direction and distances with perceptual grouping techniques (Steger *et al.* 1997). The linked edges are longer than the initial ones and are assumed to represent the borders of wind erosion obstacles or grasslands.

3.2 Edge grouping and matching

In the considered image resolution tree rows and hedges often have a left and a right border since they have a certain width in the image. So the extracted edges of two corresponding borders should be grouped into one segment. Corresponding edges can be determined by selecting one edge and searching in the cross-edge-direction within the predefined distance. The centreline of the wind erosion obstacle can be obtained by combining the edge pairs.

If no corresponding edge is found for a selected edge, the latter may be the boundary of a grassland and wind erosion obstacle. For a grassland boundary, one side is a region with a low a^* value while the other side is a homogeneous one with a high a^* value. This information is also helpful for removing grassland boundaries.

3.3 Verification with height information

After segmentation, edge extraction, grouping and matching separately both images of a stereo pair, the linear features obtained are assumed to represent the centrelines of wind erosion obstacles. Conjugate edges can be found when employing epipolar geometry and mean x -parallax. Global optimization is essential to avoid false correspondences.

To this end, the camera parameters of the stereo pair can be integrated into the extraction process. For conjugate edges, the corresponding 3-dimensional edges in object space can be obtained by forward intersection with the known camera parameters. Three-dimensional information for edges without conjugate partners in the other image can be found iteratively by taking the DSM into account: they are

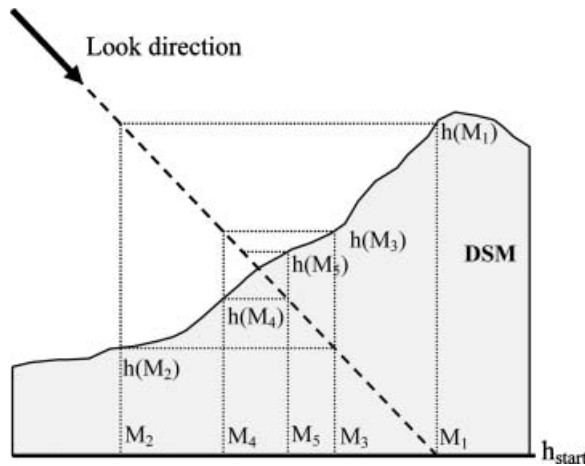


Figure 7. Height determination with a single image and a Digital Surface Model (DSM).

initially projected onto a level plane with a mean height h_{start} of the surrounding area, as shown in figure 7. The new height $h(M_1)$ can be determined from the DSM with the projected plane coordinate M_1 . Then the image edge can be projected onto a level plane with the new height $h(M_1)$ to obtain the coordinate M_2 . This recursive search procedure usually converges within a few iterations.

The resulting 3-dimensional edges are potential wind erosion obstacles. They are finally compared with the height information from the DSM to verify whether there are really wind erosion obstacles. The grassland is usually wider than the wind erosion obstacles. It exhibits a large area with nearly the same height. In this way the remaining grassland boundaries can be removed.

4. Experimental results

4.1 RGB image segmentation with CIE L^*a^*b

As mentioned above, the a^* value is negative and close to -120 for the green areas such as vegetation in standard RGB imagery, while positive and close to $+120$ for CIR imagery. Figure 8(a) shows a RGB image of Istanbul, Turkey, acquired by a digital camera in July 2004. There are sky, water, buildings and trees. Figure 8(b) is the segmented result with a threshold $a^*=12$. As can be seen, most trees remain, while the sky, water and buildings are successfully removed from the image.

Figure 9(a) is an image of Tokyo that includes cars, streets, buildings, trees and hedges. All objects other than trees and hedges are completely removed by the segmentation process with the threshold $a^*=10$, as can be seen from figure 9(b). Hedges with a width of about 1.0 m on the street, such as in the centre-left part of figure 9(b), show very strong edge structures after segmentation.

4.2 Extraction of wind erosion obstacles

The test area for the extraction of wind erosion obstacles is located in an open landscape of Lower Saxony, Germany. As mentioned in §2, GIS data, CIR stereo imagery with known camera parameters, and a DSM are used as input data. The DSM and the camera parameters of the test area are semi-automatically generated by VirtuoZo with ground control points selected from the GIS data.



Figure 8. (a) RGB image (Istanbul, Turkey) and (b) result of segmentation by CIE $L^*a^*b^*$.

The operator needs to load all the preprocessed data and predefined thresholds into the developed system and then the system runs fully automatically. It takes less than 5 minutes to extract wind erosion obstacles from a complete stereo pair with a pixel size of $100\ \mu\text{m}$ (corresponding to the mentioned ground resolution of 0.5 m) on a Pentium IV computer.

The result of vegetation extraction for a specific CIR image has already been shown in figure 6. Figure 10 depicts the edges extracted from the segmented image. For most wind erosion obstacles two corresponding edges can be seen. The edges of buildings and forests, visible for example in the centre and lower-left part of figure 10, can be masked out with the GIS data. As previously explained it is difficult to remove grassland borders, see for example the right part of figure 10, because they also appear as clear edges and exhibit a positive a^* value. Moreover, grasslands are connected to wind erosion obstacles (bottom of figure 10).

The remaining edges are linked in the along-edge-direction taking into account their direction and the gap length between two collinear edges. The linked edges are

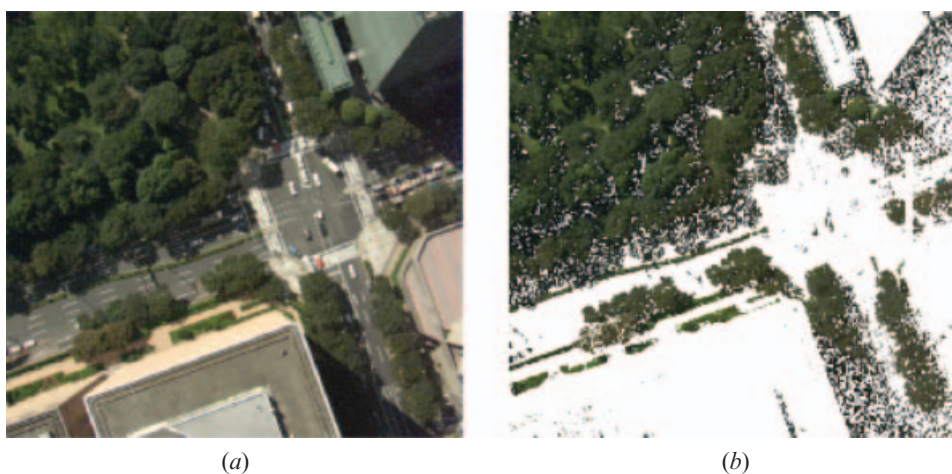


Figure 9. (a) RGB image (Tokyo, Japan) and (b) result of segmentation by CIE $L^*a^*b^*$.

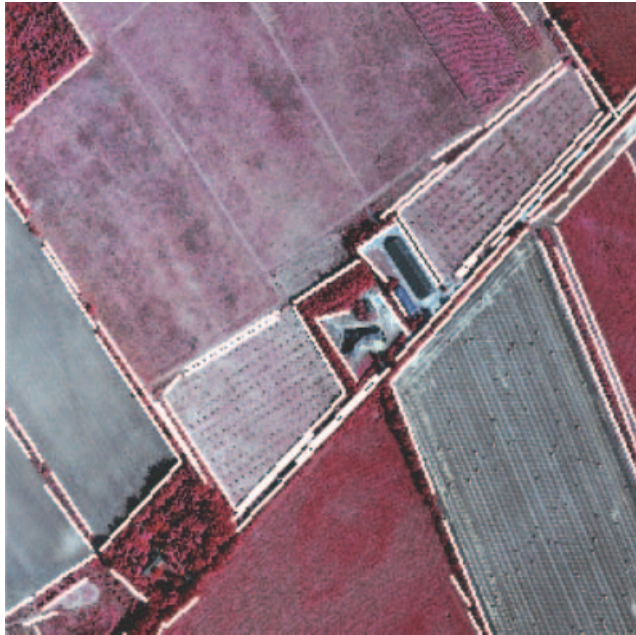


Figure 10. Extracted image edges.

longer than the initial ones and represent the borders of the wind erosion obstacles or grasslands (figure 11). Tree rows and hedges usually have two borders, and the edge pairs are derived. It can be seen in figure 12 that in the presented example all pairs are grouped successfully.

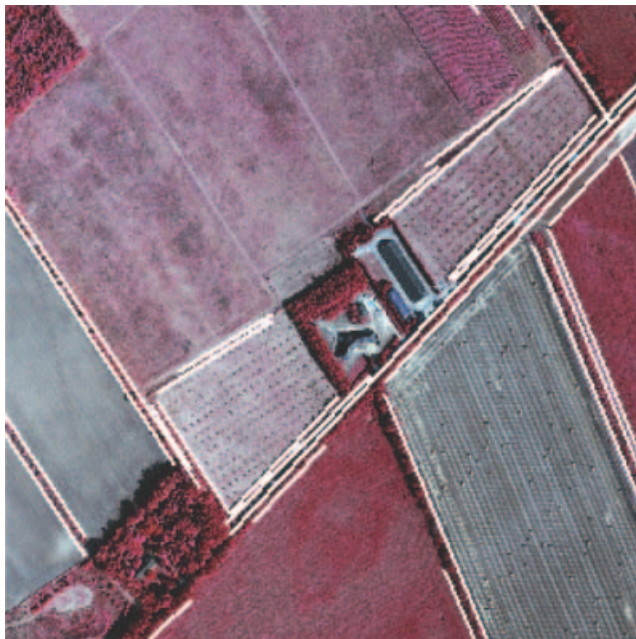


Figure 11. Linked edge segments.

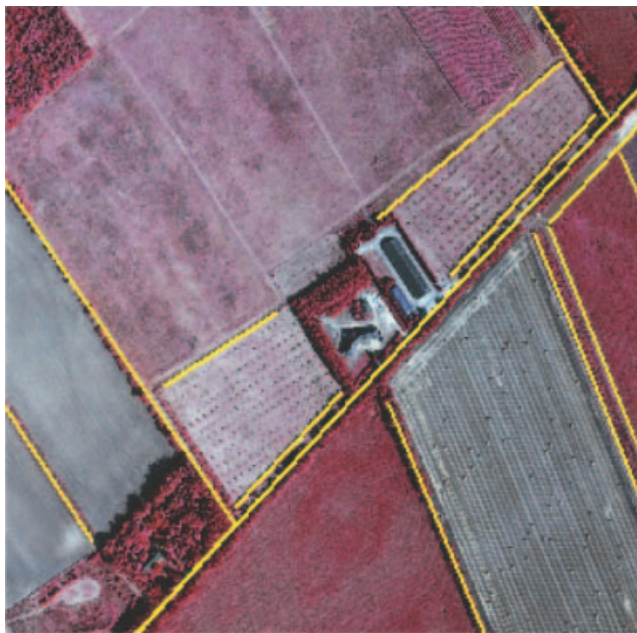


Figure 12. Grouped potential wind erosion obstacles.

Figure 13 shows the extracted wind erosion obstacles from a stereo pair after 3-dimensional verification. Most wind erosion obstacles are extracted, and only one hedge (centre of figure 13(a)) is missing. In figure 11 one can see that the edge of the missing hedge is extracted and linked successfully. This edge is grouped into the adjacent longer edge because the two are very close and the DSM information is not accurate enough.

In order to check the performance of the proposed approach in terms of completeness, correctness and geometric accuracy, all 17 wind erosion obstacles in the processed scene were also acquired manually with about 0.2m accuracy. This information is treated as reference data and compared with the extracted wind erosion obstacles. Sixteen out of the 17 wind erosion obstacles were successfully extracted, in addition the system incorrectly labelled one extracted feature as a wind erosion obstacle. The precision of planar position and the height of the extracted wind erosion obstacles are about 2.0 m and 0.5 m, respectively. This is comparable with the precision of ground control points from the GIS data.

5. Conclusions and future work

An effective approach for the extraction of wind erosion obstacles by integrating GIS data, a DSM and CIR aerial imagery is presented. In our test dataset, 16 out of 17 wind erosion obstacles were successfully extracted, and we had only one incorrect extraction. Although the dataset is limited in size, it seems that it is feasible to extract wind erosion obstacles using the described approach.

The proposed image segmentation approach by CIE L^*a^*b has good potential for the extraction of vegetation from imagery since it works on both CIR and standard RGB imagery. More investigations will be carried out to thoroughly evaluate the performance of the segmentation approach by CIE L^*a^*b , and indeed the whole

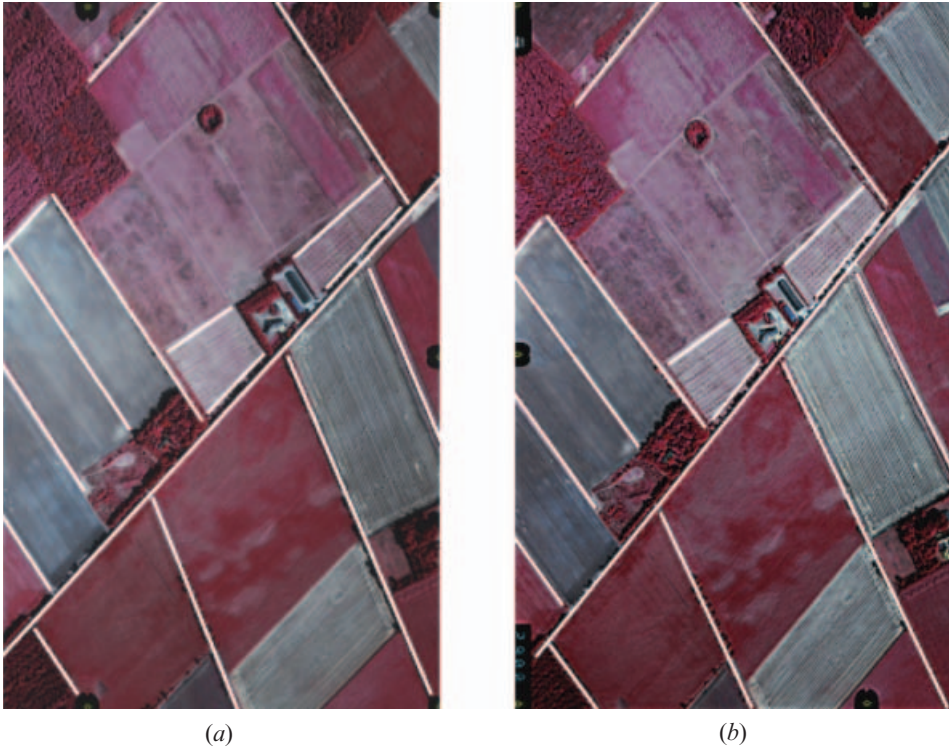


Figure 13. Extracted wind erosion obstacles from the model area of a stereo pair.

approach for extracting wind erosion obstacles from remotely sensed and aerial images.

Acknowledgments

The authors thank the anonymous reviewers for many helpful comments. This work is supported in parts by the National Natural Science Foundation of China (NSFC) under project number 40301041 and by the German GEOTECHNOLOGIEN project under contract number 03F0374A.

References

- BALTSAVIAS, E.P., 2004, Object extraction and revision by image analysis using existing geodata and knowledge: current status and steps towards operational systems. *ISPRS Journal of Photogrammetry and Remote Sensing*, **58**, pp. 129–151.
- BUTENUTH, M., 2004, Modelling the extraction of field boundaries and wind erosion obstacles from aerial imagery. *International Archives of Photogrammetry, Remote Sensing and Spatial Information Sciences*, **35**, pp. 1065–1070.
- BUTENUTH, M. and HEIPKE, C., 2005, Network snakes—supported extraction of field boundaries from imagery. In *Proceedings of the 27th DAGM Symposium*, Wien (Vienna: Springer), LNCS 3663, pp. 417–424.
- CAMPADELLI, P., SCETTINI, R. and ZUFFI, S., 2000, A system for the automatic selection of conspicuousness colour sets for qualitative data display and visual interface design. *Journal of Image and Graphics*, **5**, pp. 500–503.
- CANNY, J., 1986, A computational approach to edge detection. *IEEE Transactions on Pattern Analysis and Machine Intelligence*, **8**, pp. 679–698.

- DRALLE, K. and RUDEMO, M., 1997, Automatic estimation of individual tree positions from aerial photos. *Canadian Journal of Forest Research*, **27**, pp. 1728–1736.
- DRIEHUYZEN, M.G., 2003, Control of wind erosion. Ministry of Agriculture and Food, British Columbia, Canada. Available online at: <http://www.agf.gov.bc.ca/resmgmt/publist/600series/642200-1.pdf>.
- GOUGEON, F.A., 1995, A crown-following approach to the automatic delineation of individual tree crowns in high spatial resolution images. *Canadian Journal of Remote Sensing*, **21**, pp. 274–284.
- HEIPKE, C., PAKZAD, K. and STRAUB, B.M., 2000, Image analysis for GIS data acquisition. *The Photogrammetric Record*, **16**, pp. 963–985.
- KOUKOULAS, S. and BLACKBURN, G.A., 2005, Mapping individual tree location, height and species in broadleaved deciduous forest using airborne LiDAR and multi-spectral remotely sensed data. *International Journal of Remote Sensing*, **26**, pp. 431–455.
- LARSEN, M. and RUDEMO, M., 1998, Optimising templates for finding trees in aerial photographs. *Pattern Recognition Letters*, **19**, pp. 1153–1162.
- LEBRUN, V. and TOUSSAINT, C., 2000, On the use of image analysis for quantitative monitoring of stone alteration. Available online at: http://www.ulg.ac.be/mical/pdffiles/marble_colour_alteration.pdf.
- LUCHESE, L. and MITRA, S.K., 2001, Colour image segmentation: a state-of-the-art survey. *Proceedings of the Indian National Science Academy*, **67**, pp. 207–221.
- LYON, J.G., YUAN, D., LUNETTA, R.S. and ELVIDGE, C.D., 1998, A change detection experiment using vegetation indices. *Photogrammetric Engineering and Remote Sensing*, **64**, pp. 143–150.
- NIEDERÖST, M., 2003, Detection and reconstruction of buildings for automated map updating. Dissertation No. 14909, Eidgenössische Technische Hochschule (ETH), Zürich, Switzerland, 139 pp.
- POLLOCK, R.J., 1996, The automatic recognition of individual trees in aerial images of forests based on a synthetic tree crown image model. PhD thesis, University of British Columbia, Vancouver, Canada.
- SEII, E. M. 2002, Colors and Models. Available online at: <http://semmix.pl/color/index.html>.
- STEGER, C., MAYER, H. and RADIG, B., 1997, The role of grouping for road extraction. In *Automatic Extraction of Man-made Objects from Aerial Space Images (II)*, A. Gruen, E. Baltsavias and O. Henricsson (Eds), pp. 245–256 (Basel: Birkhäuser Verlag).
- STRAUB, B.M., 2003, Automatic extraction of trees from aerial images and surface models. *International Archives of Photogrammetry, Remote Sensing and Spatial Information Sciences*, **34**, pp. 157–164.
- SUPRESOFT 2004, Introduction of VirtuoZo system. Available online at: <http://www.supresoft.com.cn/english/products/virtuozo/virtuozo.htm>.
- UNCCD 2002, China national report to implement the United Nation's convention to combat desertification. Available online at: <http://www.unccd.int/cop/reports/asia/national/2002/china-eng.pdf>.
- WALL, G., BALDWIN, C.S. and SHELTON, I.J., 2004, Soil erosion: causes and effects. Available online at: <http://www.gov.on.ca/omafra/english/engineer/facts/87-040.htm>.
- WANG, J., RICH, P.M., PRICE, K.P. and KETTLE, W.D., 2004, Relations between NDVI and tree productivity in the central great plains. *International Journal of Remote Sensing*, **25**, pp. 3127–3138.
- WULDER, M., NIEMANN, K.O. and GOODENOUGH, D.G., 2000, Local maximum filtering for the extraction of tree locations and basal area from high spatial resolution imagery. *Remote Sensing of Environment*, **73**, pp. 103–114.
- ZHANG, Y., 2004, Extraction of wind erosion obstacles by integrating GIS-data and stereo images. *International Archives of Photogrammetry, Remote Sensing and Spatial Information Sciences*, **35**, pp. 375–380.